



## Modeling and simulation of luminescence detection platforms

Khaled Salama\*, Helmy Eltoukhy, Arjang Hassibi, Abbas El Gamal

*Department of Electrical Engineering, Stanford University, Stanford, CA 94305, USA*

### Abstract

Motivated by the design of an integrated CMOS-based detection platform, a simulation model for CCD and CMOS imager-based luminescence detection systems is developed. The model comprises four parts. The first portion models the process of photon flux generation from luminescence probes using ATP-based and luciferase label-based assay kinetics. An optics simulator is then used to compute the incident photon flux on the imaging plane for a given photon flux and system geometry. Subsequently, the output image is computed using a detailed imaging sensor model that accounts for photodetector spectral response, dark current, conversion gain, and various noise sources. Finally, signal processing algorithms are applied to the image to enhance detection reliability and hence increase the overall system throughput. To validate the model, simulation results are compared to experimental results obtained from a CCD-based system that was built to emulate the integrated CMOS-based platform.

© 2004 Elsevier B.V. All rights reserved.

*Keywords:* Luminescence probes; Modeling; CMOS sensor; Post-processing

### 1. Introduction

Conventional biological assays are highly repetitive, labor intensive, and require microliter volume samples. The associated biochemical protocols often require days or weeks to perform at a cost of hundreds of dollars per test. Problems remain in detecting and quantifying low levels of biological compounds reliably, conveniently, safely and quickly. There is also a growing interest in the development of inexpensive portable biosensors for environmental and biomedical diagnostics. Solving these problems will require the development of new techniques and sensors, not only to selectively identify target compounds, but also to assay large numbers of samples.

A biochemical testing procedure can be divided into four steps: sample preparation, assay, detection, and data analysis as shown in Fig. 1. Currently, each step is being separately automated and miniaturized. However, there continues to be a need for designs that accommodate efficient integrated circuit manufacturing techniques to realize associated cost savings. We have been investigating the integration of three

of these four steps into a single miniaturized platform as shown Fig. 2.

A variety of assay methods have been developed for molecular detection. These methods include electrochemistry (Woolley et al., 1998), optical absorption (Kunz, 1997), interferometry (Verpoorte et al., 1992), luminescence and fluorescence (Haugland, 1998). In this paper we focused on luminescence detection or luminometry. This technique is becoming increasingly popular due to its high sensitivity, wide dynamic range, and relatively inexpensive instrumentation. Superior sensitivity and low background distinguish luminometry from other analytical methods. Luminometry is up to five orders of magnitude more sensitive than absorption spectroscopy and more than 1000 times more sensitive than fluorometry. A state-of-the-art luminometer can detect as little as 0.6 pg of adenosine triphosphate (ATP) or 0.1 fg of luciferase (~1100 molecules), two common luminescent analytes (Turner et al., 1985). Numerous bioluminescent and chemiluminescent reactions are studied using luminometry and are commonly used in biotechnology research, environmental testing, industrial applications, and clinical research. Among its many applications are the measurements of gene expression using reporter gene assays, the determination of intracellular ATP, and DNA sequencing.

Commercially available platforms for photon detection use bulky CCD camera-based setups and require the use of large quantities of reagents due to the light loss in the

\* Corresponding author. Present address: Packard 257, 350 Serra Mall, Stanford, CA 94305, USA. Tel.: +1-650-725-9696; fax: +1-650-724-3648.

*E-mail address:* [knsalama@stanford.edu](mailto:knsalama@stanford.edu) (K. Salama).

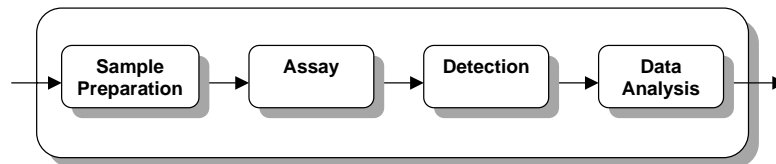


Fig. 1. General system currently used for biochemical testing.

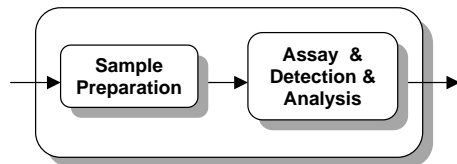


Fig. 2. Proposed system for future biochemical testing.

acts upon a luminescent probe. The second category is indirect or linked detection in which the luminescent species indirectly measures the targeted characteristic, usually through an intermediate chemical process (Tang et al., 1995; Koster et al., 1997; Van Dyke et al., 2002; De Mello, 1996). While multiplexing is feasible in direct target detection, indirect detection requires confinement of the photon generation process as well as physical barriers for the independent reactions. This physical isolation complicates the integration of indirect detection methods to miniaturized systems, since high density mechanical barriers (e.g. micro-wells) as well as micro-scale solution delivery systems would be required. Since indirect detection is the more general of the two categories, it is the focus of the following analysis.

### 2.1. Luminescence light generation

The time-dependent light generation from a typical luminescence process is a function of the underlying chemical reaction kinetics. The rate of a reaction, in general, is the speed at which reactants are converted into products. If enzyme species  $E$  (the catalyst) converts the substrate molecule  $S$  into product  $P$ , the stoichiometric formula is given by



where  $k_f$  and  $k_r$  are the association and disassociation rate constants. In (1) the reaction rate is defined by

$$\text{rate} = \frac{d[P]}{dt} = -\frac{d[S]}{dt} = k_f[S][E] - k_r[E][P], \quad (2)$$

where  $[E]$ ,  $[S]$ , and  $[P]$  are the concentrations of the enzyme, substrate and product in the medium, respectively. Now if we suppose that the above process is a luminescence enzymatic reaction with quantum yield  $\alpha$ , then the photon generation rate  $I$  in volume  $V$  of the reaction medium ( $A$  is Avogadro's number) would 'be

$$I = (\alpha VA) \frac{d[P]}{dt} = (\alpha VA)[E](k_f[S] - k_r[P]). \quad (3)$$

The total number of photons generated by this luminescence process  $N_{\text{ph}}(T)$ , in the time interval  $T$ , would be

$$N_{\text{ph}}(T) = (\alpha VA)[E] \int_T (k_f[S] - k_r[P]) dt. \quad (4)$$

In luminescence assays the experiment is typically set up in such a way that the luminescence probe (e.g. a light generating enzyme) either reports the quantity of a substrate molecule (e.g. ATP) or the molecule to which it binds (e.g.

optical path. As a result these systems are not well suited to low cost applications. The development of imaging sensors in standard complementary metal-oxide-semiconductor (CMOS) technologies makes it possible to integrate sensing and processing on the same integrated circuit, enabling many low power and low cost applications. We have designed an integrated CMOS-based detection platform for use with luminescent microarrays. (Eltoukhy et al., 2004) A major concern in the design of such a miniaturized system is that the photogenerated signals can be very weak and therefore difficult to detect reliably. To quantify the detection limits of the envisioned system for the required assay concentration and throughput, we built a complete model for simulating the path from photogeneration through the optical path to detection and image post processing. Such modeling is used to guide the overall system design, whereby the special characteristics of a wide array of luminescent assaying methods can be exploited to enhance detection sensitivity beyond that of off-the-shelf CCD or CMOS-based sensors.

In Section 2, we describe the light generation process of luminescent probes and formulate the complete kinetic model of ATP-based and luciferase label-based assays. In Section 3, we describe the model of the proposed luminescent detection system including the associated optical pathway, imaging array characteristics, and applied signal processing algorithms. Finally, in Section 4, we present simulation and experimental results.

## 2. Luminescence light generation processes

Luminescence assay techniques are divided into two general categories. The first is direct target detection in which the photon emitting species physically interacts with the target of interest at a predetermined location. An example of this approach is luminescence-based immunoassays, which usually involve probing a protein of interest with a primary antibody that reacts with a secondary antibody. Light is produced when the enzyme bound to the secondary antibody

140 luciferase-based labels in immunoassays). The photon gen-  
 141 eration rate from the luminescence reaction, which is a func-  
 142 tion of the target concentration, is then measured and corre-  
 143 lated to the target concentration.

144 2.1.1. Substrate detection kinetics

145 In the first group of luminescence assays, the rate at which  
 146 photons are generated represents the substrate concentration  
 147 given by (3). As the substrate is consumed by the catalyst,  
 148 the light intensity decreases and eventually approaches zero.  
 149 If we assume that the disassociation rate is insignificant (i.e.  
 150 negligible inhibition), the light intensity with initial substrate  
 151 concentration  $[S_0]$  becomes

152 
$$I(t) = (\alpha VA) \frac{d[P(t)]}{dt} = (\alpha VA) k_f [E][S_0] e^{-k_f [E]t}. \quad (5)$$

153 The total amount of photons from time  $t = 0$ , the start of  
 154 the process, to  $t = T$  is

155 
$$N_{ph}(T) = (\alpha VA)[S_0](1 - e^{-k_f [E]T}). \quad (6)$$

156 The photon intensity in (6) is proportional to the target  
 157 concentration, but the light intensity decays exponentially  
 158 with a time constant, which is a function of the catalyst  
 159 concentration and turnover rate  $k_f$ .

160 2.1.2. Catalyst detection kinetics

161 The second approach in luminescence assays is to link  
 162 the target molecule quantity to a luminescence catalyst. In  
 163 this approach, excess substrate is used, making sure that  
 164 its consumption does not affect the reaction kinetics. If the  
 165 saturation concentration for the substrate is  $[S_{max}]$  and the  
 166 target concentration is equal to the catalyst  $[E]$ , the light  
 167 intensity becomes

168 
$$I(t) = (\alpha VA) \frac{d[P(t)]}{dt} = (\alpha VA) k_f [S_{max}][E]. \quad (7)$$

169 Since the light intensity based on (7) is time independent  
 170 and proportional to the target (or the catalyst) concentration,  
 171 the total number of photons generated from this process is  
 172 a function of the integration time, i.e.

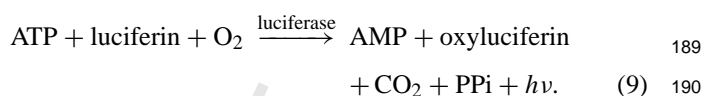
173 
$$N_{ph} = (\alpha VA) k_f [S_{max}][E]T. \quad (8)$$

174 In such assays, the number of target molecules can be very  
 175 small resulting in a low but steady light. Long integration  
 176 times, however, can be used to collect a significant number  
 177 of photons.

2.2. Models of specific luminescent assays

2.2.1. ATP measurement

180 ATP bioluminescence assays are designed to measure  
 181 the quantity of adenosine 5'-triphosphate (ATP) in a sam-  
 182 ple (Scheda et al., 1995). Its applications include indirect  
 183 measurement of bacteria, yeasts, fungi and other mi-  
 184 croorganisms, which have a regulated number of ATP in  
 185 foodstuffs, beverages, water and other media. The assay  
 186 typically employs recombinant luciferase to catalyze the  
 187 reaction



191 In most practical assays, the concentration of luciferin is  
 192 high enough that we can consider it to be in deep saturation  
 193 as shown in Fig. 3a. In this case, and when product inhi-  
 194 bition is negligible, the rate of ATP consumption is given  
 195 by

196 
$$\frac{d[\text{ATP}]}{dt} = -k_L [E][\text{luciferin}_{max}][\text{ATP}] e^{-k_f [E][\text{luciferin}_{mac}]t}, \quad (10)$$

199 where  $k_L$  is the association rate of luciferase macro-reaction.  
 200 We can rewrite (10) by substituting  $k_t = k_L [E][\text{luciferin}_{max}]$   
 201 as the turnover rate of the ATP consumption to obtain

202 
$$I(t) = (\alpha VA) k_t [\text{ATP}] e^{-k_t t}. \quad (11)$$

203 The quantum efficiency of luciferase is about 0.88, and  
 204 the turnover rate of the enzyme, depending on the ratio of  
 205 luciferase to ATP, can vary from 0.1 to  $1 \text{ s}^{-1}$  (glow com-  
 206 pared to flash). In the glow process, the light intensity is  
 207 approximated by

208 
$$I(t) \approx 5.3 \times 10^{22} V[\text{ATP}_0] e^{-0.1t}. \quad (12)$$

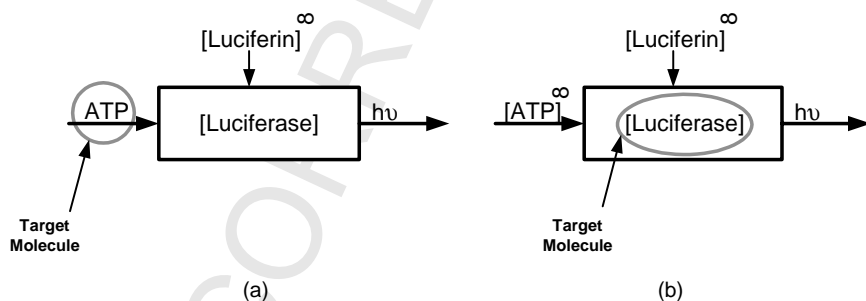


Fig. 3. Block diagram of (a) ATP detection assay and (b) luciferase detection system. The ( $\infty$ ) symbol indicates excess concentration.

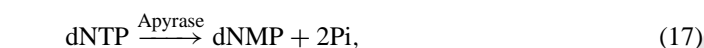
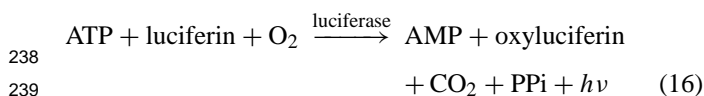
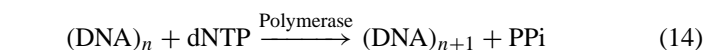
209 2.2.2. Luminescent labels

210 If the reporter of a specific biological process is the cata-  
 211 lyst of a luminescence reaction, the assay can be optimized  
 212 in such a way that the rate-limiting factor becomes the cat-  
 213 alyst concentration (Kricka, 1988). In such an assay, any  
 214 change in target concentration changes the catalyst concen-  
 215 tration, therefore altering the photon flux intensity as shown  
 216 in Fig. 3b. The light intensity in the case where luciferase  
 217 is the label of the target becomes

218  $I(t) \approx 5.3 \times 10^{22} V[E_0].$  (13)

219 2.2.3. Pyrosequencing

220 Pyrosequencing is a DNA sequencing method based on  
 221 the detection of released inorganic pyrophosphate during  
 222 DNA synthesis. Using a linked enzymatic reaction, visible  
 223 light (at 562 nm) proportional to the number of incorporated  
 224 nucleotides is generated (Brovko et al., 1994; Ronaghi et al.,  
 225 1996; Ronaghi, 2001). The enzymatic cascade begins with a  
 226 DNA polymerization reaction in which inorganic pyrophos-  
 227 phate (PPi) is released as a result of nucleotide incorporation  
 228 by polymerase. The released PPi is subsequently converted  
 229 to ATP by ATP-sulfurylase. The synthesized ATP provides  
 230 the energy for luciferase to generate photons. Unincorporated  
 231 deoxy-nucleotides and ATP are degraded by the en-  
 232 zyme apyrase to chemically reset the enzymatic system af-  
 233 ter the incorporation test. The enzymatic reactions in this  
 234 method are given by



242 where APS is adenosine phosphosulfate, AMP, adenosine  
 243 monophosphate, dNTP, deoxynucleotide triphosphate, and

244 Pi, phosphate. As shown in Fig. 4 this enzymatic system  
 245 regulates the light generation by recycling PPi, but the de-  
 246 grading enzyme, apyrase, breaks all nucleotide and ATP  
 247 molecules in time, thus decreasing the light intensity. If we  
 248 assume that PPi regulation has a unity gain positive feed-  
 249 back, and the turnover rate of apyrase is  $k_a$ , then the light  
 250 generated by single incorporation from this bioluminomet-  
 251 ric assay is

252  $I(t) = (\alpha VA)k_t[DNA]e^{-k_a t}.$  (18)

253 For most practical applications,  $k_a \approx 0.05 \text{ s}^{-1}$  and  $k_t \approx$   
 254  $1 \text{ s}^{-1}$ , and thus the light intensity becomes

255  $I(t) = 5.3 \times 10^{23} V[DNA]e^{-0.05t}.$  (19)

256 In (19) the negative effects of product inhibition are not  
 257 included. While these unwanted pathways can potentially  
 258 alter the kinetics of the reaction and the light intensity in  
 259 general, one can still approximate light intensity in cases in  
 260 which the sample concentration is low.

261 3. Detection system modeling

262 Having established a comprehensive model for the quan-  
 263 tum efficiency of bioluminometric assays, we now discuss  
 264 the detection portion of the system. Various detection  
 265 systems have been developed for luminometry. By far  
 266 the most sensitive detection devices are photomultiplier  
 267 tubes (PMTs), which via a photocathode and a series of  
 268 amplifying dynodes can generate up to one million elec-  
 269 trons for every incident photon. These devices are very  
 270 sensitive since their noise can be removed easily using a  
 271 level-discriminator. However, they are costly and require  
 272 high operating voltages (1000 VDC), precluding their use  
 273 in a portable system. Furthermore, the overall photon de-  
 274 tection efficiency of PMT-based systems is limited to 1–4%  
 275 by the optics and the low quantum efficiency (10%) of  
 276 PMTs. Finally, multiplexed imaging is not readily feasible  
 277 using PMT's, as they are relatively large and thus unsuit-  
 278 able for dense arrays. It is this aspect of PMT's that has  
 279 most limited their use and applicability (Van Dyke et al.,  
 280 2002).

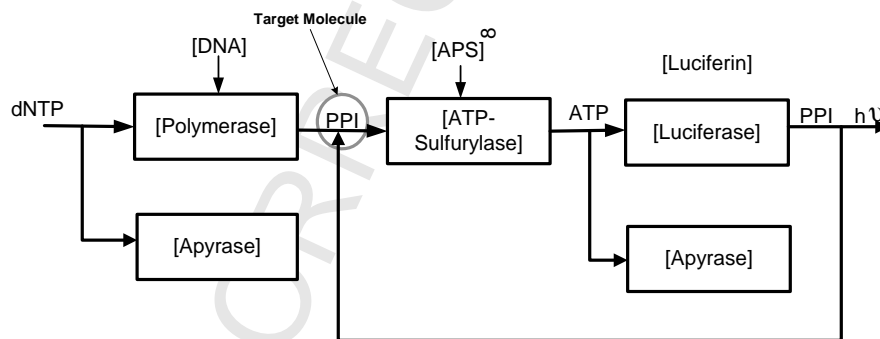


Fig. 4. Block diagram of pyrosequencing in which PPi released from DNA polymerization is measured. The (∞) symbol corresponds to excess concentration. Apyrase competes with polymerase and luciferase for dNTP and ATP consumption.



281 The most commonly used visible range imaging sensor  
 282 architectures employ either charge-coupled device (CCD) or  
 283 CMOS photosensor arrays. The major difference between  
 284 the two is the specific readout mechanism used. CCDs em-  
 285 ploy a “bucket brigade” to serially shift out the photogener-  
 286 ated electrons accumulated at each photosite. CCDs are fab-  
 287 ricated in a nonstandard semiconductor process that is solely  
 288 optimized for sensing and charge transfer (Holst, 1991).  
 289 As a result, CCD image sensors achieve very high sensi-  
 290 tivity, low noise, and low non-uniformity; hence they have  
 291 earned a central place in the biological imaging arena. Al-  
 292 though PMTs are more sensitive, unfortunately it has been  
 293 our experience that ensuring the reliability of the chem-  
 294 istry itself places the true lower bound on detection re-  
 295 quirements and thus CCDs do not have practical deficien-  
 296 cies in this respect. Since the thermal and shot noise gen-  
 297 erated from the photodiode junction cannot be differentiat-  
 298 ed from the photogenerated signal, cooling the device is  
 299 the primary means of reducing such noise to negligible lev-  
 300 els. Although liquid nitrogen is used in applications requir-  
 301 ing extreme sensitivity (77 K), a lower cost and typically  
 302 adequate solution involves incorporating a stack of Peltiers  
 303 to cool the sensor down to as low as 200 K. This, how-  
 304 ever, requires the use of several high supply voltages result-  
 305 ing in high power consumption. Moreover, no other analog  
 306 or digital circuits, such as for clock generation, timing,  
 307 analog-to-digital (A/D) conversion, digital processing and  
 308 storage, can be integrated with a CCD image sensor on a sin-  
 309 gle chip resulting in multi-chip imaging system implemen-  
 310 tations with high power consumption, high cost, and large  
 311 size.

312 CMOS, on the other hand, offers the benefits of CCDs  
 313 with the possibilities of circumventing many of their draw-  
 314 backs. For instance, CMOS offers complete customizability  
 315 of the photodetection array to suit the requirements of the  
 316 specific biological application. Hence the detection area of  
 317 each photodiode can be optimally sized with respect to the  
 318 assay volume and its light generation characteristics. Fur-  
 319 thermore, this quality allows one to forego intermediary op-  
 320 tics and to perform “contact” photonic detection of chemilu-

321 minescent assay signals, thereby drastically increasing pho-  
 322 todetection efficiency to near  $QE$  limited percentages while  
 323 eliminating expensive and bulky optics. This improvement  
 324 alone can increase sensitivity of the system by an order of  
 325 magnitude. Although others (Eggers et al., 1994; Lamture  
 326 et al., 1994) performed such detection using a CCD-based  
 327 sensor, it is the leveraged use of an integrated CMOS pro-  
 328 cess that leads to considerable overall gains in system per-  
 329 formance. More specifically, CMOS makes true low power  
 330 operation possible, with the ability to integrate both the ADC  
 331 and the DSP on chip enabling high quality detection combin-  
 332 ed with incomparable portability (El Gamal et al., 1999).  
 333 Intelligent use of CMOS circuitry can be used to compen-  
 334 sate for non-idealities engendered by the poorer quality (rel-  
 335 ative to CCDs) of added noise from the readout chain. In-  
 336 clusion of transparent on-chip background subtraction and  
 337 signal averaging circuitry are two examples that can help  
 338 improve CMOS detection quality beyond that of CCD’s.  
 339 Background subtraction removes the deterministic thermally  
 340 generated portion of the photodiode signal, leaving only its  
 341 shot noise component that has a variance equal to the square  
 342 root of its mean. Signal averaging lowers the independent  
 343 noise components by  $\sqrt{n}$ , where  $n$  is the number of indepen-  
 344 dent samples. Indeed, using CMOS as a biological platform  
 345 has the potential of making “in the field” biological testing a  
 346 reality.

347 A conceptual schematic of the proposed integrated sys-  
 348 tem in which the chemistry is directly coupled to the  
 349 CMOS-based detection chip is shown in Fig. 5a. A block  
 350 diagram of the proposed detection chip is shown in Fig. 5b.  
 351 It consists of a 2D array of pixels, each containing a pho-  
 352 todetector and transistors for readout. The collected charge  
 353 from each pixel is read out and converted in parallel to a  
 354 digital format via an array of per-pixel analog-to-digital con-  
 355 verters (ADCs). The system includes memory for on-chip  
 356 storage of multiple frames. Moreover, a dedicated digital  
 357 signal processor (DSP) is integrated on the chip to perform  
 358 any needed computations, such as for background subtrac-  
 359 tion and read noise reduction. A detailed description of a  
 360 prototype is provided in (Eltoukhy et al., 2004).

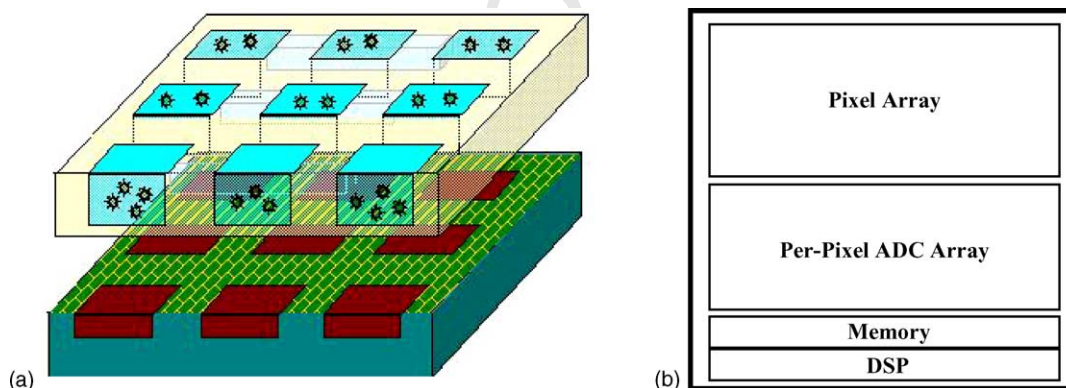


Fig. 5. (a) Conceptual schematic of the proposed integrated platform demonstrating the tight coupling between the sensor array and the biological assay reactions and (b) block diagram of the detection chip showing its main components.

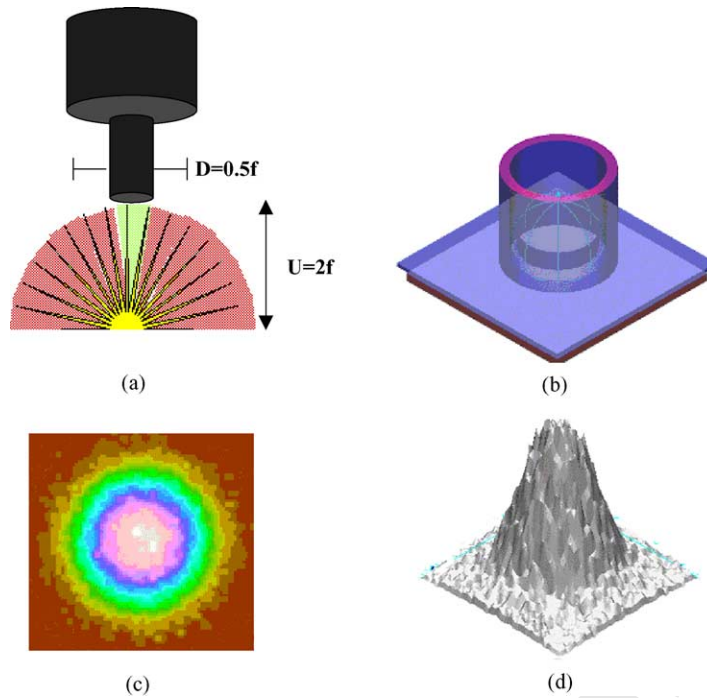


Fig. 6. (a) Model of light loss in camera-based system, (b) optical model of sensor-coupled assay, (c) simulated 2D sensor-plane intensity distribution, and (d) 3D sensor-plane intensity distribution.

360 In Sections 3.1, 3.2 and 3.3 we describe the modeling  
 361 and algorithms involved in the optics, image sensor and  
 362 post-processing components of the detection chain.

363 3.1. Optics model

364 We first compare the optical efficiency of direct coupling  
 365 to a conventional camera-based imaging system. Assuming  
 366 that the object to be imaged is a point source located a  
 367 distance  $U$  away from the lens (or the imaging surface in  
 368 the case of direct coupling), the numerical aperture NA of  
 369 the object side can be approximated using geometric optics  
 370 by  $\sin(\theta_{max})$ , where  $\theta_{max} = \tan^{-1}(D/2U)$  where  $D$  is the  
 371 diameter of the lens aperture. Since optical efficiency (i.e.

fraction of light collected by the lens) is proportional to  
 372  $(NA)^2$ , the efficiency of a camera-based system (see Fig. 373  
 374 6a) for typical parameter values of  $D = 0.5 f$  and  $U = 2 f$ ,  
 375 where  $f$ , the focal length is a mere 1.6%. Optical efficiency  
 376 can be greatly improved by directly coupling the chemistry  
 377 to the detection chip surface as proposed in our integrated  
 378 system. For example, taking  $D = 100 \mu m$  (photodetector  
 379 size) and  $U = 15 \mu m$ , the optical efficiency becomes 91%.

To accurately compute the optical efficiency for the  
 380 direct coupling scenario, we use an optical simulator  
 381 (LightTools™) and the specific luminescent assay and sensor  
 382 parameters of the proposed setup to compute the point  
 383 spread function, PSF (i.e. the function describing the distri-  
 384 bution of light at the imaging plane due to a point source

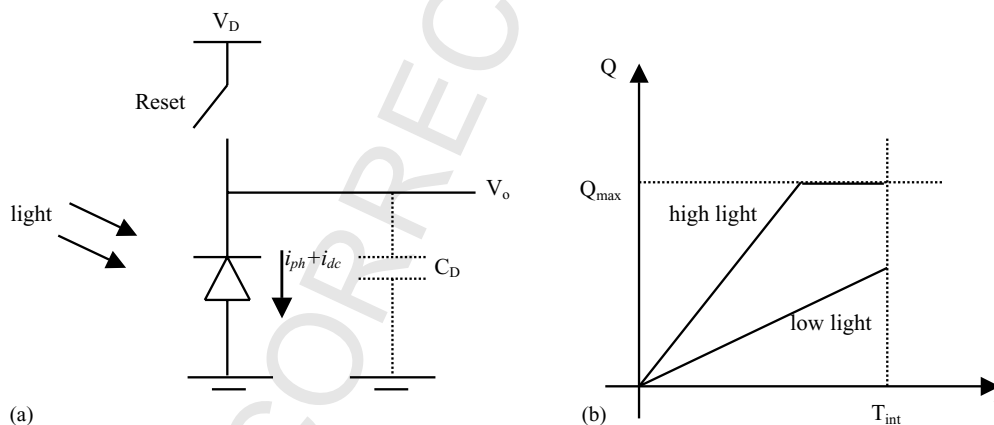


Fig. 7. (a) Simplified photodiode pixel model and (b) photocharge vs. time under different illumination conditions.

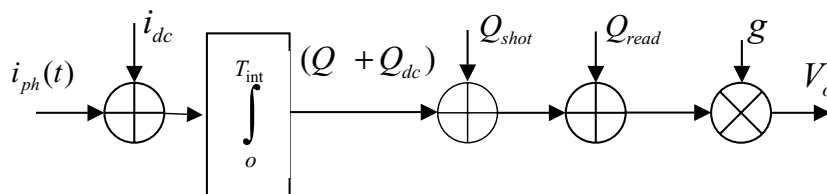


Fig. 8. Image sensor model, including added dark current, shot and read noises.

385 at the object plane). The PSF relates to the degree of blur-  
 386 ring encountered in an optical system and can be used to  
 387 calculate the resultant light intensity at the image plane due  
 388 to the finite separation distance between the assay and the  
 389 sensor. This is performed by convolving the derived PSF  
 390 with the intensity distribution at the object plane to obtain  
 391 the corresponding distribution at the imaging plane. Fig. 6b  
 392 depicts a simplified model of the imaging setup and the  
 393 simulated intensity distribution at the sensor plane is plotted  
 394 in Figs. 6c and d.

395 **3.2. Image sensor model**

396 An image sensor comprises an array of pixels each having  
 397 a photodetector and devices for readout. The sensor is typ-  
 398 ically operated in direct integration as illustrated in Fig. 7.  
 399 Photons incident on the photodetector are converted into  
 400 photocurrent. The photocurrent is directly integrated over  
 401 the photodiode capacitance  $C_D$  into charge  $Q$ . The amount  
 402 of charge that can be collected is limited by the well cap-  
 403 acity  $Q_{max}$ . At the end of integration time  $T_{int}$ , the charge  
 404 is read out as a voltage signal  $V_o$ , which is related to  $Q$   
 405 by the conversion gain  $g$ , i.e.  $V_o = gQ$ . Fig. 8 summarizes the  
 406 overall image sensor model, including dark current, added  
 407 shot and read noise, and the conversion gain.

408 The efficiency of converting incident photons to photocur-  
 409 rent  $i_{ph}(t)$  is governed by the spectral response  $\eta(\lambda)$  of the  
 410 detector, where  $\lambda$  is the emission wavelength, and is given  
 411 by

412 
$$i_{ph}(t) = \eta(\lambda)I_{incident}(t). \quad (20)$$

413 Several sources contribute to noise during the collection  
 414 of the photogenerated signal including dark current  $i_{dc}$  and  
 415 photocurrent shot noise, reset noise, and readout noise. The  
 416 total added average noise power can be expressed as

417 
$$\sigma_n^2 = \frac{1}{q}(Q + Q_{dc}) + Q_{read}^2, \quad (21)$$

418 where the first term is the average power of the integrated  
 419 shot noise of both the signal and the dark current,  $Q_{read}^2$  is  
 420 the average read noise power, and  $q = 1.602 \times 10^{-19}$  C.  
 421 The signal-to-noise ratio, SNR, is defined as the ratio of the  
 422 photogenerated signal power to the noise power and is given  
 423 by

424 
$$SNR = \frac{Q^2}{\sigma_n^2}. \quad (22)$$

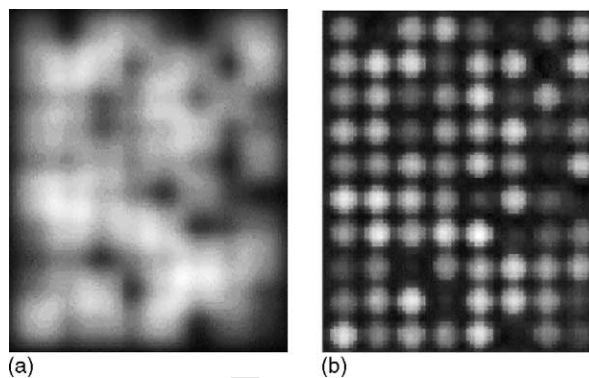


Fig. 9. Microarray image (a) before post-processing and (b) after applying cross-talk reduction algorithm.

425 **3.3. Image post-processing**

426 Once the image data is collected, post-processing algo-  
 427 rithms can be applied to correct for non-idealities in both  
 428 the optics and image sensor. For instance, the PSF can be  
 429 used to correct for assay cross-talk using conventional equal-  
 430 ization techniques, such as Weiner filtering. This enables  
 431 higher throughput for the detection system, since tighter as-  
 432 say pitches can be tolerated. Fig. 9 shows an example of this  
 433 filtering technique on an image with excessive cross-talk.  
 434 Additionally, subtraction of both the chemical and detector  
 435 backgrounds as well as digital accumulation incorporating  
 436 the reaction kinetics can be performed to enhance SNR and,  
 437 thus, detection reliability.

438 **4. Simulation and experimental results**

439 By combining the models and algorithms discussed in  
 440 the previous sections for the reaction kinetics, optical path,  
 441 image sensor and post-processing, the minimum detectable  
 442 analyte concentration can be estimated for a given set of  
 443 detection system parameters. A block diagram of the lumi-  
 444 nescence detection system simulator that implements these  
 445 models is shown in Fig. 10. The simulator, including the re-  
 446 action kinetics and image sensor models, are coded in Mat-  
 447 lab, while the optical efficiency and PSF for a given system  
 448 geometry are calculated using LightTools™ and passed as  
 449 arguments to the Matlab script.

450 To validate the above simulation model, we built an iso-  
 451 lated imaging chamber for luminescence detection. The sys-

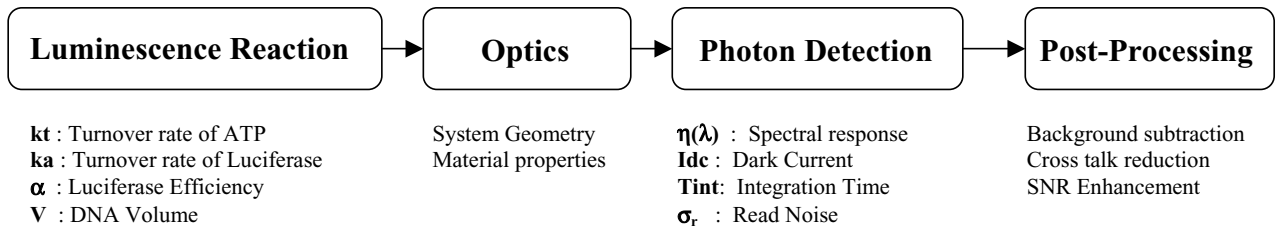


Fig. 10. Block diagram of luminescence detection system simulator.

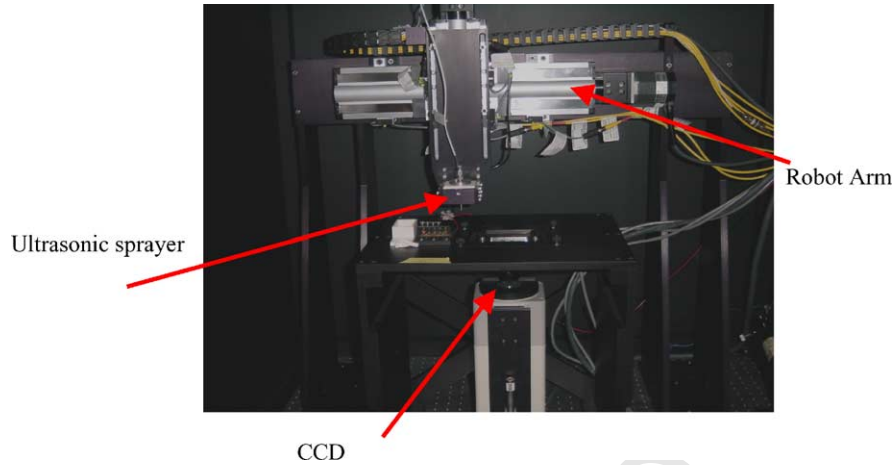


Fig. 11. Image of the prototype system including a robot-arm, an ultrasonic sprayer and a cooled CCD sensor.

452 tem employs an ultrasonic sprayer attached to a robotic  
 453 arm for nucleotide and enzyme delivery to the target assays  
 454 above the imaging apparatus as shown in Fig. 11. In order to  
 455 simulate the types of conditions that would be encountered

in an integrated CMOS detection system, a scientific-grade  
 CCD (Hamamatsu HC230) is incorporated with the ultra-  
 sonic sprayer. The system allows direct placement of the  
 assay slide onto the CCD. The CCD output is connected to

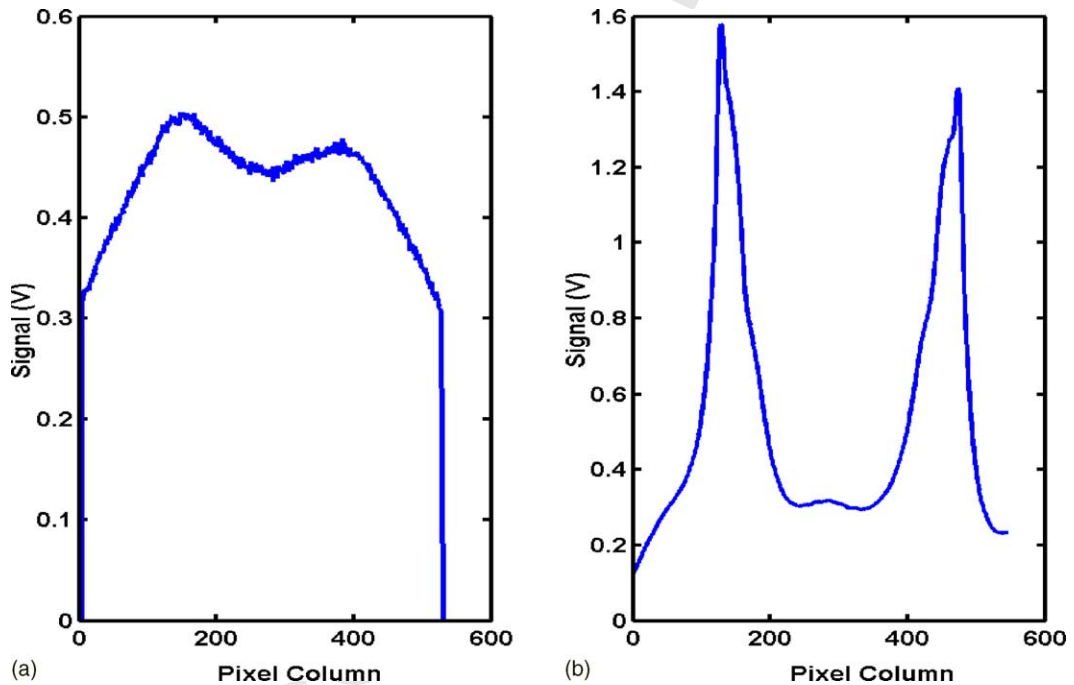


Fig. 12. (a) Plot of measured output signal voltage from each column of the CCD array for two adjacent 0.1 pmol wells and (b) same output after applying signal processing algorithms to reduce the effect of the system PSF.



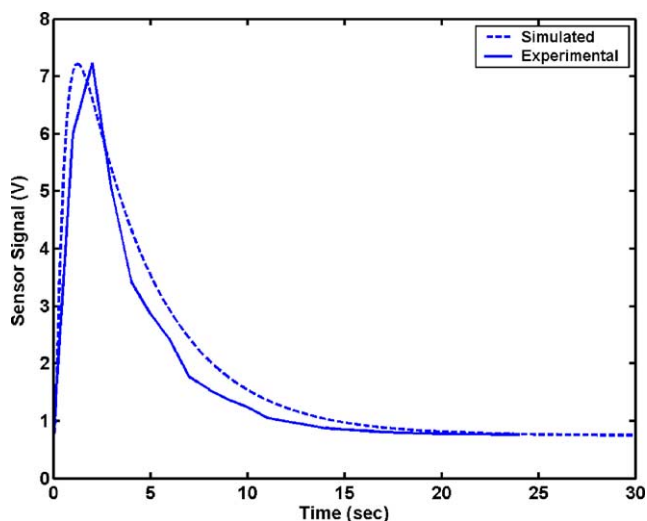


Fig. 13. Experimental data vs. combined chemistry and sensor simulation of detected signal vs. time of nucleotide incorporation in a Pyrosequencing reaction.

a dedicated PC for simultaneously controlling the robotic arm of the sprayer, capturing images, and processing the assay data to achieve accurate detection. We implemented a simple but efficient algorithm for signal detection that can run in parallel with the data acquisition software. The algorithm automatically performs background subtraction of noise and utilizes line binning to increase SNR. An eight-tap low pass filter is utilized to smooth the resultant signal and remove any high frequency noise components. Also integrated with the script is an equalization routine for reduction of cross-talk using the modeled system PSF (see Fig. 12). This experimental setup allows for accurate measurement of the quantum efficiency of the reaction as well as of the optical and detection paths. The overall system dimensions are 50 cm × 50 cm × 60 cm due to the presence of the robotic arm. In contrast, the envisioned CMOS system under development will measure 10 cm × 10 cm × 2 cm.

We have used the experimental system to measure the light intensity produced during the incorporation of a single base in a Pyrosequencing reaction. Using 100 fmol of DNA per well, which is 10-fold lower than the amount currently used in commercial Pyrosequencing systems, we measured a peak signal-to-noise ratio of 750. We have also used the collected experimental data to fine-tune the parameters of the chemical kinetics, optics, and detector models. This “tuning” involved incorporating the specific association and disassociation rate constants, optical path loss, sensor noise characteristics, and overall system delay resulting from the finite mixing time of the sprayer. Fig. 13 compares the simulated and experimental results during incorporation of one nucleotide in a Pyrosequencing reaction using 100 fmol of DNA. As is readily seen, the simulation results are fairly well corroborated by the experimental data. Furthermore, using typical CMOS process parameter values at room temperature, our model predicts that 0.5 photon/s/μm<sup>2</sup> in con-

junction with  $T_{\text{int}} = 10$  s and 100 μm × 100 μm diode sizes would be needed to achieve a signal-to-noise ratio of 10. This implies that an integrated CMOS-based luminescence detection system would be capable of performing pyrosequencing with as little as 1 fmol of DNA, an amount three orders of magnitude lower than current commercial machines.

## 5. Conclusion

We described a simulation model for CCD and CMOS-based luminescence detection platforms. The model quantifies the photon flux generated by luminescence probes using ATP-based and luciferase label-based assay kinetics. The photon flux coupled with the system geometry is then used to calculate the incident photon flux on the imaging plane. Subsequently, the output image is computed using a detailed image sensor model. We constructed a prototype system to experimentally verify the developed models. Using this experimental setup we are able to obtain accurate measurements of the quantum efficiency, temporal kinetics and spatial distribution of the reaction, which are used to calculate the optimal assay sizes and throughput limits for the CMOS-based system.

## Acknowledgements

The authors wish to thank Dr. M. Ronaghi, Dr. P. Griffin, Prof. R. Davis, A. Agah, A. Ercan, and S. Kavusi for their valuable insight and helpful discussions. We acknowledge the support of the Stanford Genome Technology Center in conducting most of the experimental work.

## References

- Brovko, L., Gandel'man, O., Polenova, T., Ugarova, N., 1994. Kinetics of bioluminescence in the firefly luciferin–luciferase System. *Biochemistry* 59, 195–201.
- De Mello, A.J., 1996. *Surface Analytical Technique for Probing Biomaterial Processes*. CRC Press, Boca Raton/New York.
- El Gamal, A., Yang, D., Fowler, B., 1999. Pixel-level processing—why, what and how. *Proceedings of the SPIE* 5650, pp. 2–13.
- Eltoukhy, H., Salama, K., El Gamal, A., Ronaghi, M., Davis, R.W., 2004. A 0.18 μm CMOS 10<sup>-16</sup> lux bioluminescence detection SoC. *IEEE ISSCC Digest of Technical Papers* 47.
- Eggers, M., Hogan, M., Reich, R., Lamture, J., Ehrlich, D., Hollis, M., Kosicki, B., Powdrill, T., Beattie, K., Smith, S., Varma, R., Gangadharan, R., Mallik, A., Burke, B., Wallace, D., 1994. A microchip for quantitative detection of molecules utilizing luminescent and radioisotope reporter groups. *Biotechniques* 17 (3), 516–525.
- Haugland, R.P., 1998. *Handbook of Fluorescent Probes and Research Chemicals, Molecular Probes*. Eugene, OR.
- Holst, G., 1991. *CCD Arrays, Cameras, and Displays*, 2nd edition, SPIE Press.
- Koster, H., Van Den Boom, D., Braun, A., Jacob, A., Jurinke, C., Little, D.P., Tang, K., 1997. DNA analysis by mass spectrometry: applications in DNA sequencing and DNA diagnostics. *Nucleosides Nucleotides* 16, 563–571.

- 545 Kricka, L.J., 1988. Clinical and biological applications of luciferases and  
546 luciferins. *Anal. Biochem.* 175, 14–22.
- 547 Kunz, R.E., 1997. Miniature integrated optical modules for chemical and  
548 biochemical sensing. *Sens. Actuators B* 38, 13–28.
- 549 Lamture, J.B., Beattie, K.L., Burke, B.E., Eggers, M.D., Ehrlich, D.J.,  
550 Fowler, R., Hollis, M.A., Kosicki, B.B., Reich, R.K., Smith, S.R.,  
551 1994. Direct detection of nucleic acid hybridization on the sur-  
552 face of a charge coupled device. *Nucl. Acids Res.* 22 (11), 2121–  
553 2125.
- 554 Ronaghi, M., Karamohamed, S., Pettersson, B., Uhlen, M., Nyren, P.,  
555 1996. Real-time DNA sequencing using detection of pyrophosphate  
556 release. *Anal. Biochem.* 242, 84–89.
- 557 Ronaghi, M., 2001. Pyrosequencing sheds light on DNA sequencing.  
558 *Genome Res.* 11, 3–11.
- 559 Schena, M., Shalon, D., Davis, R.W., Brown, P.O., 1995. Quantitative  
560 monitoring of gene expression patterns with a cDNA microarray.  
*Science* 270, 467–470.
- Tang, K., Fu, D., Kotter, S., Cotter, R.J., Cantor, C.R., Koster, H., 1995. 561  
Matrix-assisted laser desorption/ionization mass spectrometry of im- 562  
mobilized duplex DNA probes. *Nucl. Acids Res.* 23, 3126–3131. 563
- Turner, G.K., 1985. Measurement of light from chemical or biochemical 564  
reactions. In: Van Dyke, N., Van Dyke, C., Woodfork, K., (Eds.), Bio- 565  
luminescence and Chemiluminescence: Instruments and Applications, 566  
pp. 43–78. 567
- Van Dyke, N., Van Dyke, C., Woodfork, K., (Eds.), 2002. Luminescence 568  
Biotechnology: Instruments and Applications. CEC Press, Boca Ra- 569  
ton/New York. 570
- Verpoorte, E., Manz, A., Ludi, H., Bruno, A.E., Maystre, F., Krattiger, B., 571  
Widmer, H.M., Van Der Schoot, B.H., De Rooij, N.F., 1992. A silicon 572  
flow cell for optical-detection in miniaturized total chemical-analysis 573  
systems. *Sens. Actuators B* 66 (6), 66–70. 574
- Woolley, A.T., Lao, K., Glazer, A., Mathies, R.A., 1998. Capillary elec- 575  
trophoresis chips with integrated electrochemical detection. *Anal.* 576  
*Chem.* 70, 684–688. 577

UNCORRECTED PROOF